COMPUTER METHODS AND PROGRAMS IN BIOMEDICINE 138 (2017) 1–12

journal homepage: www.intl.elsevierhealth.com/journals/cmpb

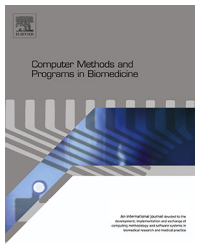

Individual tooth segmentation from CT images scanned with contacts of maxillary and mandible teeth

Zeyang Xia [a,b,1,*], *Yangzhou Gan* [a,b,1], *Lichao Chang* [a], *Jing Xiong* [a,*], *Qunfei Zhao* [c]

[a] *Shenzhen Institutes of Advanced Technology, Chinese Academy of Sciences, Shenzhen, China*
[b] *CAS Key Laboratory of Human-Machine Intelligence-Synergy Systems, Shenzhen Institutes of Advanced Technology, Shenzhen, China*
[c] *Shanghai Key Lab of Navigation and Location Services, and Department of Automation, Shanghai Jiao Tong University, Shanghai, China*

ARTICLE INFO

Article history:
Received 31 January 2016
Received in revised form
13 August 2016
Accepted 4 October 2016

Keywords:
Computed tomography images
Tooth segmentation
Radon transform
Level set method
Mesh segmentation

ABSTRACT

Background and objective: Tooth segmentation from computed tomography (CT) images is a fundamental step in generating the three-dimensional models of tooth for computer-aided orthodontic treatment. Individual tooth segmentation from CT images scanned with contacts of maxillary and mandible teeth is especially challenging, and no method has been reported previously. This study aimed to develop a method for individual tooth segmentation from these images.

Methods: Tooth contours of maxilla and mandible are first segmented from the volumetric CT images slice-by-slice. For each slice, a line is extracted using the Radon transform to separate neighboring teeth, and each tooth contour is then segmented by a level set model from the corresponding side of the line. Then, each maxillary tooth whose contours overlap with that of mandible ones is detected, and a mesh model is reconstructed from all the contours of these maxillary and mandible teeth with contour overlap. The reconstructed mesh model is segmented using threshold and fast marching watershed method to separate the touched maxillary and mandible teeth. Finally, the separated tooth models are restored to fill the holes to obtain complete tooth models. The proposed method was tested on CT images of ten subjects scanned with natural contacts of maxillary and mandible teeth.

Results: For all the tested images, individual tooth regions are extracted successfully, and the segmentation accuracy and efficiency of the proposed method is promising.

Conclusions: The proposed method is effective to segment individual tooth from CT images scanned with contacts of maxillary and mandible teeth.

© 2016 Elsevier Ireland Ltd. All rights reserved.

* *Corresponding author.* 1068 Xueyuan Avenue, Shenzhen University Town, Shenzhen 518055, China.
E-mail addresses: zy.xia@siat.ac.cn (Z. Xia), jing.xiong@siat.ac.cn (J. Xiong).

[1] These authors contributed equally to this work.

http://dx.doi.org/10.1016/j.cmpb.2016.10.002
0169-2607/© 2016 Elsevier Ireland Ltd. All rights reserved.

1. Introduction

Individual three-dimensional (3D) models of tooth are needed for the computer-aided orthodontic treatment planning and simulation [1]. Tooth segmentation from computed tomography (CT) images is a fundamental step in the modeling of tooth.

In the past decades, several methods have been proposed to segment teeth from CT images scanned while the subjects' teeth are in an open bite position where the maxillary and mandible teeth have no contact. These methods can be classified into two classes: 3D segmentation and two-dimensional (2D) slice-by-slice segmentation. The 3D segmentation methods directly segment tooth region in the 3D volumetric space. Akhoondali et al. [2] developed an automatic segmentation method based on region growing. Keyhaninejad et al. [3] and Hosntalab et al. [4] proposed to use 3D region based level set model to extract the tooth surface. Keustermans et al. [5] and Hiew et al. [6] applied a graph cut algorithm to interactively segment 3D tooth volume. Barone et al. [7] developed a novel framework to iteratively model the 3D shape of tooth with single-root from CT images. Instead of directly segmenting tooth from the volumetric images, they outlined the 2D contours of target tooth from a set of projected images, and the 3D tooth shape was modeled from these contours using a B-spline representation.

The 2D slice-by-slice segmentation methods segment tooth contours in each slice. This kind of methods generally applies the similarity of tooth intensity and/or shapes between adjacent slices to automatically initialize the tooth region, and the user only needs to manually initialize a starting slice. Heo and Chae [8] and Wu et al. [9] used the B-spline snakes with genetic algorithm to extract tooth contours. The B-spline snakes used in their methods cannot address the topological change of tooth contours. The level set method has been broadly used for the tooth contour segmentation due to its advantages in dealing with topological change and contour propagation [10–13]. Gao and Chae [10] proposed a level set model with shape and intensity prior to segment the tooth and achieved promising results. Yau et al. [11] applied the same model to extract the root contours. Ji et al. [12] modified this model to segment the anterior teeth. In our previous work [13], a hybrid level set model was developed for accurate root segmentation.

In orthodontics, the treatment not only needs to align teeth in each jaw, but also requires the teeth of maxilla and mandible to maintain correct occlusion condition. To check the occlusion condition, the dental CT images often needs to be scanned while the subjects' teeth are in a close bite position where maxillary and mandible teeth contact naturally. In these images, tooth contours of maxilla and mandible overlap in some slices of the occlusal contact area. The previous tooth segmentation methods are infeasible to extract individual tooth region from these images due to the missing boundaries between mandible and maxillary teeth. Wang et al. [14,15] proposed promising methods to segment maxilla and mandible from CT images scanned with contacts of maxillary and mandible teeth. However, there did not involve the individual tooth segmentation from alveolar bone.

The main contribution of this study is to develop a method for individual tooth segmentation from CT images scanned with contacts of maxillary and mandible teeth. The developed method first segments tooth contours from the volumetric CT images slice-by-slice using level set method. Then, each maxillary tooth whose contours overlap with that of mandible ones is detected, and a mesh model is reconstructed from all the contours of these maxillary and mandible teeth with contour overlap. The reconstructed model is segmented by threshold and fast marching watershed method to separate the contacted maxillary and mandible teeth. Finally, the separated tooth models are restored to fill the holes, and complete models of individual tooth are obtained.

The remainder of the manuscript is organized as follows. Section 2 introduces the background of the level set method and mesh model segmentation method. Section 3 presents the proposed individual tooth segmentation method. Section 4 shows the experimental results and discussions of the method, and the manuscript is concluded in Section 5.

2. Background of the level set method and mesh model segmentation

2.1. Hybrid level set model

The level set method is increasingly applied to medical image segmentation [16,17]. Recently, a hybrid level set model [13] was developed to segment tooth from CT image scanned without contact of maxillary and mandible teeth and presented excellent segmentation accuracy. The hybrid level set model is composed of a global intensity energy, a local intensity energy, a tooth shape constraint energy, and an edge detection energy. In this model, the global and local intensity energy are employed to address the topological changes and drive the curve move rapidly toward tooth boundary. The edge detection energy is integrated into the level set length regularization term to smooth and refine the localization of the curve. The tooth shape constraint term is used to constrain the tooth contour evolving toward the prior shape. The energy function of the hybrid level set model is expressed as follows

$$E(\phi) = (1-w)E_{global}(\phi) + wE_{local}(\phi) + \beta E_{shape}(\phi) + \mu E_{edge}(\phi) \quad (1)$$

where ϕ is a 2D level set function, E_{global}, E_{local}, E_{shape}, and E_{edge} denote the global intensity energy, local intensity energy, tooth shape constraint energy, and edge detection energy, respectively; $\omega \in (0, 1)$, β, and μ are positive constants, representing the weight parameters of the corresponding energy term.

Let $\Omega \in \Re^2$ be the image plane, $I{:}\Omega \to \Re$ be the given gray image to be segmented, and Ω_1 ($\phi \geq 0$) and Ω_2 ($\phi < 0$) be the foreground and background regions, respectively, the global intensity energy is defined as

$$E_{global}(\phi) = \int_{\Omega} \log\left(\frac{p(I(X)|\Omega_2)}{p(I(X)|\Omega_1)}\right) H_\varepsilon(\phi(X))\,dx \quad (2)$$

where $p(I(X)|\Omega_i)$ ($i = 1, 2$) denotes the conditional probability of the intensity value $I(X)$ ($X \in \Re^2$), H_ε is the normalized Heaviside function [18]. The conditional probability $p(I(X)|\Omega_i)$ is estimated from the previous segmented slice.

The local intensity energy comes from the local Gaussian distribution fitting energy [19], and is written as

$$E_{local}(\phi) = \int_\Omega \left(\int_\Omega K_\sigma(X-Y) \left(\frac{|I(Y)-f_1(X)|^2}{2\sigma_1(X)^2} + \log\sigma_1(X) \right) H(\phi(Y)) dY \right) dX + \int_\Omega \left(\int_\Omega K_\sigma(X-Y) \left(\frac{|I(Y)-f_2(X)|^2}{2\sigma_2(X)^2} + \log\sigma_2(X) \right) (1-H(\phi(Y))) dY \right) dX \quad (3)$$

where K_σ is a Gaussian kernel with a scale parameter σ, $f_1(X)$ and $f_2(X)$ are the local mean intensities in Ω_1 and Ω_2, respectively, and σ_1 and σ_2 are the corresponding standard variances.

The tooth shape constraint energy is defined as the dissimilarity of the current tooth shape and the prior tooth shape [20], and is written as

$$E_{Shape}(\phi) = \int (H_\varepsilon(\phi(X)) - H_\varepsilon(\phi_0(X)))^2 dX \quad (4)$$

where ϕ_0 is the signed distance function which embeds the prior tooth shape, and comes from the segmented tooth contour of the previous slice.

The edge detection energy is integrated into the level set length regularization term to smooth and refine the localization of the curve, and is written as

$$E_{edge} = \int_\Omega g\delta_\varepsilon(\phi)|\nabla\phi| dX \quad (5)$$

where g is the edge indicator with gradient direction detection [21], and is defined as

$$g(x) = \begin{cases} \dfrac{1}{1+|\nabla G_s * I(X)|^2}, & \nabla G_s * I\phi_0 \geq 0 \\ 1, & \nabla G_s * I\phi_0 < 0 \end{cases} \quad (6)$$

where $G_s * I$ denotes the smoothed version of I by convolving I with the Gaussian kernel G_s, and ∇ denotes the differential operator. Thus, the energy function of the hybrid level set model is written as

$$E_{hybrid}(\phi) = (1-\omega)\int \log\left(\frac{p(I|\Omega_1)}{p(I|\Omega_2)}\right) H_\varepsilon(\phi) dX + \omega \sum_{i=1,2} \int_\Omega \left(\int_\Omega K_\sigma(X-Y) \left(\frac{|I(Y)-f_i(X)|^2}{2\sigma_i(X)^2} + \log\sigma_i(X) \right) M_i(\phi) dY \right) dX + \beta\int (H_\varepsilon(\phi)-H_\varepsilon(\phi_0))^2 dX + \mu\int_\Omega g\delta_\varepsilon(\phi)|\nabla\phi| dX \quad (7)$$

where $M_1(\phi) = H\varepsilon(\phi)$, and $M_2(\phi) = 1 - H\varepsilon(\phi)$. The minimization of Eq. (7) can be achieved by an explicit iteration from the following gradient descent flows

$$\frac{\partial\phi}{\partial t} = \delta_\varepsilon(\phi)\left[\omega \sum_{i=1,2} (-1)^i \int_\Omega K_\sigma(X-Y) \left(\frac{|I(Y)-f_i(X)|^2}{2\sigma_i(X)^2} + \log\sigma_i(X) \right) dY - (1-\omega)\log\left(\frac{p(I|\Omega_1)}{p(I|\Omega_2)}\right) - 2\beta(H_\varepsilon(\phi)-H_\varepsilon(\phi_0)) + \mu div\left(g\frac{\nabla\phi}{|\nabla\phi|} \right) \right] \quad (8)$$

where $t > 0$ is the artificial iterative time, and $div(\bullet)$ denotes the divergence operator.

2.2. Mesh segmentation

A 3D mesh model M is a set which consists of the face set F and the vertex set V, and $M = \{F, V\}$. The goal of mesh segmentation is to decompose a mesh into smaller and meaningful sub-meshes. Lots of methods have been developed for mesh segmentation, including region growing, watershed algorithm, and spectral analysis and so on. When the segmentation object is given, whatever algorithm is used, the most important factor affecting the result is the criteria to decide which elements belong to the same part. These criteria are always based on the attributes extracted from the mesh [22]. Two of the most useful attributes in various methods are the curvature and average geodesic distance.

2.2.1. Curvature estimation

There are many variations for curvature calculation. One of the most important curvature is the Gaussian curvature and can be estimated using Meyer method [23]. Using the Meyer method, the Gaussian curvature k_G of vertex v is calculated by the following expression

$$k_G(v)=\frac{1}{A_M}\left(2\pi-\sum_{i\in N(v)}\theta_i\right) \tag{9}$$

where $N(v)$ denotes all the 1-neighborhood vertexes of v, θ_i is the angle of the i-th face at the vertex v, A_M denotes the Voronoi area of the vertex v which sums areas of partial region of the adjacent triangles for the whole 1-neighborhoods. More details on the computation of Voronoi area can be found in Ref. [23].

The directly computed Gaussian curvature in Eq. (9) is not always accurate to obtain satisfying segmentation and can be improved by employing the mean shift method [24]. Given a data set of Gaussian curvatures, the mean-shift method first estimates the density function of the curvatures. Then, it calculates the gradient of the density function and moves the curvature along gradient direction. Given the vertexes and curvatures, the mean shift density function is written as:

$$f(k_G(v))=\frac{1}{|V|h}\sum_{v_i\in N_2(v)}K\left(\frac{k_G(v)-k_G(v_i)}{h}\right) \tag{10}$$

where $K(\bullet)$ denotes the kernel function, h is the corresponding bandwidth, $|V|$ is the total number of vertexes, and $N_2(v)$ denotes the 2-neighboring vertexes of v. Let $K(\bullet)=pk(\|\bullet\|^2)$, where p is a normalization constant making the integration of $K(\bullet)$ to be 1, and $k(x)$ is the profile function. The gradient of density function (10) is written as:

$$\nabla f(k_G(v))=\frac{2p}{|V|h^3}\left[\sum_{v_j\in N_2(v)}g\left(\left\|\frac{k_G(v)-k_G(v_j)}{h}\right\|^2\right)\right]m(k_G(v)) \tag{11}$$

where $g(\bullet)=-k'(\bullet)$, and $m(k_G(v))$ is the mean-shift vector written as

$$m(k_G(v))=-k_G(v)+\sum_{v_i\in N_2(v)}k_G(v)g\left(\left\|\frac{k_G(v)-k_G(v_i)}{h}\right\|^2\right)\Bigg/\sum_{v_i\in N_2(v)}g\left(\left\|\frac{k_G(v)-k_G(v_i)}{h}\right\|^2\right) \tag{12}$$

The mean shift iteration procedure of the Gaussian curvature $k_G(v)$ is implemented through the gradient-ascent process

$$k_G(v)^{t+1}=k_G(v)^t+m\left(k_G(v)^t\right),\quad t=0,1,2,\ldots \tag{13}$$

The iteration process (13) stops until the change of $k_G(v)$ is lower than a given value (for example 10exp4).

2.2.2. *Average geodesic distance*

The average geodesic distance of a given vertex represents the means of geodesic distance from the vertex to all other vertexes on the mesh, and is calculated as follows:

$$A(v_i)=\frac{1}{N}\sum_{j=1}^{N}geod(v_i,v_j) \tag{14}$$

where $geod(v_i,v_j)$ is the geodesic distance between vertexes v_i and v_j, and N denotes the number of vertexes on the mesh. The geodesic distance between two vertexes can be calculated using Dijsktra algorithm.

2.2.3. *Fast marching watershed algorithm for mesh segmentation*

The fast marching watershed algorithm [25] is inspired from fast marching method [26] and watershed algorithm. Its segmentation procedure is similar to a downhill process. The unlabeled vertexes in the mesh can be labeled through downhill process from high to low according to a height function. Given a height function, the procedure of the fast marching watershed algorithm is conducted by the following steps:

Step 1. Given the vertex set V, the corresponding height function H, an array L labeling unlabeled 1-neighborhoods of labeled vertexes;
Step 2. Find all the un-labeled 1-neighborhoods of the labeled vertexes, and put these vertexes into L;
Step 3. Sort the vertexes in L according to the height function in descending order;
Step 4. Label the first vertex in L according to its labeled 1-neighborhoods, and remove it from L.
Step 5. Find all the un-labeled 1-neighborhoods of the removed vertex in step 4, and put all the found vertexes into L;
Step 6. Go back to step 3 unless L is empty.

3. Proposed method

3.1. *Overview*

The procedure of the proposed method for individual tooth segmentation from CT images scanned with contacts of maxillary and mandible teeth is shown in Fig. 1. The segmentation procedure consists of three steps: (*I*) user initialization, (*II*) tooth contour segmentation, and (*III*) mesh model segmentation.

In step *I*, a user manually selects a starting slice for each jaw and picks a seed point for each tooth in the selected starting slices. For each jaw, the starting slice is selected from crown part near the tooth neck where all tooth contours are included and no alveolar bone connects with tooth. It divides the volumetric images of the jaw into crown and root slices.

In step *II*, tooth contours are segmented slice-by-slice automatically. Tooth segmentation of each jaw is conducted independently. For each single jaw, the segmentation starts from the starting slice and propagates along the crown and root directions for crown and root segmentation using a tooth contour propagation strategy. The tooth contour propagation strategy applies segmented tooth contour of the previous slice as tooth shape prior to initialize and guide the segmentation of the current slice. In the segmentation of each slice, the Radon transform is used to extract a line to separate neighboring tooth contours, and the hybrid level set model is then employed to segment each tooth contour from the corresponding side of the line.

In step *III*, each maxillary tooth whose contours overlap with that of the mandible ones is detected, and a model is reconstructed from all the contours of these maxillary and mandible teeth with contour overlap. The reconstructed model is generally composed of one maxillary tooth and two or one mandible teeth. It is then segmented by a threshold segmentation and fast marching watershed method to separate the

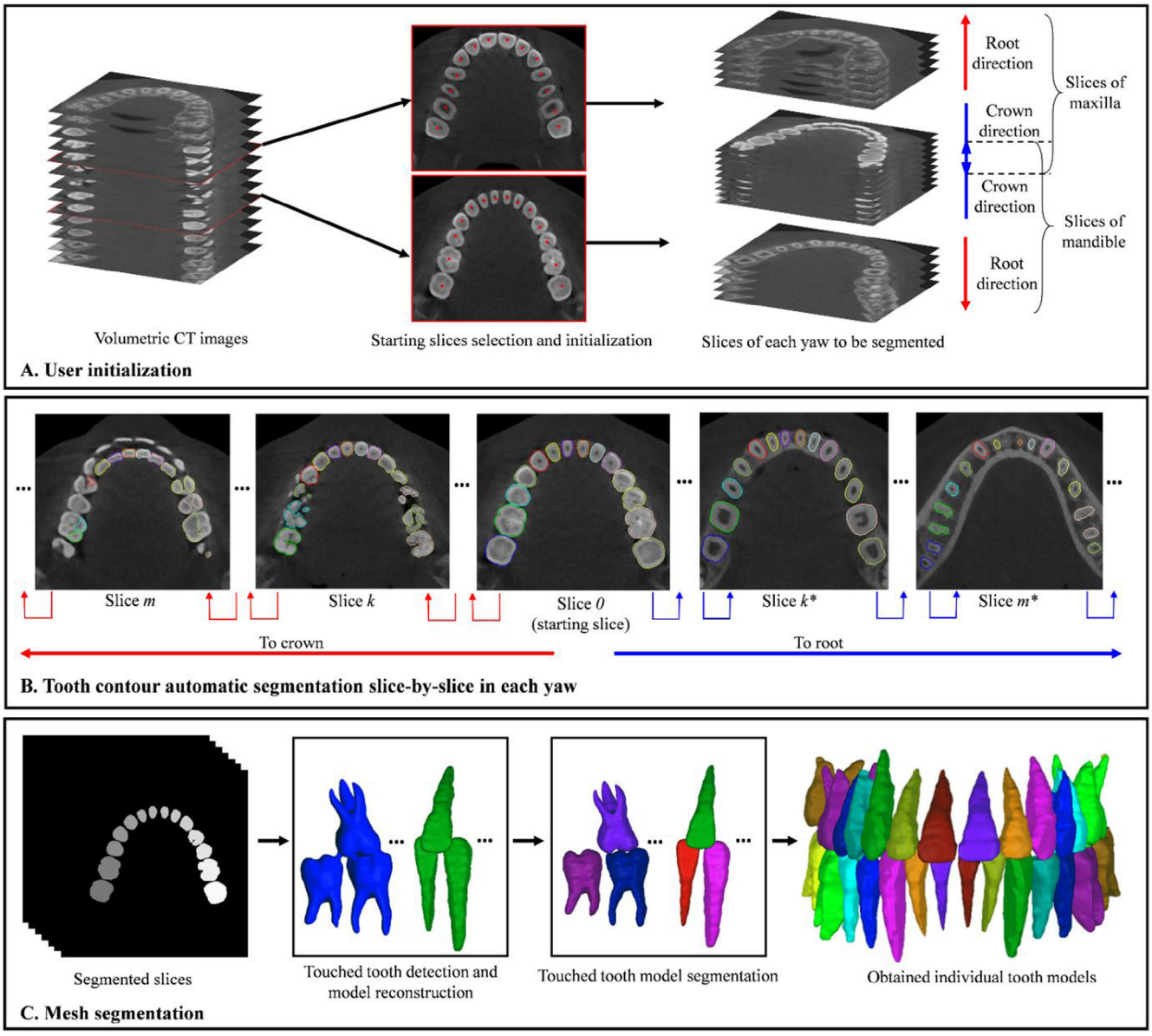

Fig. 1 – Procedure of individual tooth segmentation from CT images scanned with contacts of maxillary and mandible teeth.

maxillary and mandible teeth. The separated tooth models are finally restored to fill holes, and complete individual tooth models can be obtained.

3.2. *Tooth contour segmentation*

Neighboring teeth especially in crown part may touch each other such that the common boundary in between are missing, and segmentation algorithm may consider the two teeth as one and fail to extract individual tooth contour. In order to extract individual tooth contour from each slice, this study first applies the Radon Transform to compute a line to separate neighboring teeth into independent ones, then uses the hybrid level set model to segment each tooth from the corresponding side of the line.

3.2.1. *Separation line extraction of neighboring teeth using the Radon transform*

The Radon transform of a given image $I(x_1, x_2)$ ($x_1, x_2 \in \Re$) represents a collection of one-dimensional line integral (i.e. projection) in various directions:

$$R(\theta, \rho)(I(x_1, x_2)) = \int_{-\infty}^{+\infty}\int_{-\infty}^{+\infty} I(x_1, x_2)\delta(\rho - x_1\cos\theta - x_2\sin\theta)dx_1dx_2 \quad (15)$$

where θ denotes the angle between the perpendicular direction of line integral and the x_1-axis, and ρ denotes the perpendicular offset of the line integral.

The separation line of neighboring teeth corresponds to a local minimum point $R(\theta_0, \rho_0)$ in the Radon transform as the image projection along the line reaches a local minimum. Given the reference shapes (the initial contours) of neighboring teeth

to be separated, the local minimum point $R(\theta_0, \rho_0)$ needs to satisfy two constraint conditions. (1) θ_0 should approximate to α, the angle of the major axis of the connected contour of reference shapes obtained by dilating the reference shapes using a disk shaped structuring element with diameter of 5 pixels (the dilation operation generally has little effect on the angle of the major axis), such that the separation line remains approximately perpendicular to the dental arch ($\theta_0 \in [\alpha - 30°, \alpha + 30°]$ in this study). (2) ρ_0 needs to be bounded within the perpendicular offset of centroids of the reference shapes. Before the separation line extraction, the reference shapes of neighboring teeth are dilated to check whether the neighboring teeth are in close proximity to each other. Only when the dilated shapes intersect, separation line extraction procedure would be conducted. In addition, the Radon transform of each pair of neighboring teeth is calculated from pixels within the connected contour.

3.2.2. *Modification to the hybrid level set model*

In the hybrid level set model (7), three parameters whose values will affect the results need to be tuned manually. This study develops an adaptive parameter estimation scheme to determine the weight parameter ω and β from the image data, and only the parameter μ is selected manually for the model to adapt different images.

For the pixel whose statistical model is clear to be foreground or background, the global intensity energy should be dominant to guide the level set evolving quickly, and ω should have a small value. While for the pixel whose statistical model is ambiguous, the local intensity energy should be dominant to drive the level set curve move toward the tooth boundary, and ω should have a large value. Thus, in order to achieve the best performance, the weight parameter ω needs to adaptively adjust according to the image intensity distribution. This study uses the following expression to estimate its value

$$\omega = 4p(\Omega_1|I)\,p(\Omega_2|I) \approx 4p(I|\Omega_1)\,p(I|\Omega_2) \tag{16}$$

In Eq. (16), when $p(\Omega_i|I)$ is close to 1 or 0, the statistic model, whether the pixel is in the foreground or background, is clear and $1 - \omega$ approximates to its maximum 1 which means the global intensity energy is dominant. When $p(\Omega_i|I)$ is close to 0.5, the statistic model, whether the pixel is in the foreground or background, is ambiguous, and ω approximates to its maximum 1 which means the local intensity energy is dominant.

The prior shape constraint energy (4) does not involve any image data, and the constraint does not favor any pixels. Ideally, the prior shape constraint energy should have a strong constraint force at the weak boundary and have a weak constraint force at the strong boundary. The image intensity of tooth is generally higher than that of other tissues. Inside the zero level set curve, the higher intensity a pixel has, the more unlikely it is to be a boundary. Thus, inside the zero level set curve, the shape constraint force should be strong for the pixel with high intensity and weak for the pixel with low intensity. While outside the zero level set curve, the lower intensity a pixel has, the more unlikely it is to be a boundary. Thus, outside the zero level set curve, the shape constraint force should be strong for the pixel with low intensity and weak for the pixel with high intensity. Additionally, the farther from the initial contour the pixel is, the more unlikely it is to be the boundary. Thus, the prior shape constraint force should be strong for pixel far from the initial contour and be weak for pixel near the initial contour. For this purpose, the parameter β is adaptively estimated by:

$$\beta = (1 - \delta_\varepsilon(\phi_0))(H_\varepsilon(\phi)I_N + (1 - H_\varepsilon(\phi))(1 - I_N)) \tag{17}$$

where I_N denotes the normalized version of I whose maximum is normalized to 1.

3.3. *Mesh model segmentation for contacted maxillary and mandible tooth separation*

The segmented contours of maxillary and mandible teeth may overlap in some slices. It is infeasible to reconstruct correct individual tooth models from these overlapped contours. To obtain individual tooth models, this study first detects the touched maxillary and mandible teeth and reconstructs their 3D mesh models. Then, the reconstructed mesh model is segmented to separate the touched maxillary and mandible teeth.

3.3.1. *Contacted tooth detection and model reconstruction*

There are multiple maxillary teeth that need to be separated from mandible teeth if directly modeling the teeth from all the segmented contours. It is a challenging work to automatically separate multiple touched teeth. As neighboring tooth contours in each jaw have been separated in the tooth contour segmentation step, this study sequentially takes each maxillary tooth as the object, and then detects the mandible teeth that touched with it. In the segmented contours of a given maxillary tooth, if there is overlap with contours of any mandible teeth, it is regarded that this given maxillary tooth contacts with some mandible teeth. Then, a mesh model is reconstructed from all contours of the given maxillary tooth and the contacted mandible teeth with contour overlap using Marching Cube algorithm [27]. As the touched areas of maxillary and mandible teeth are always located at the occlusal contact area in the crown part, the mesh model is reconstructed from contours of the crown part. The reconstructed model is generally composed of one given maxillary tooth and two or one mandible teeth.

3.3.2. *Mesh model segmentation*

Fig. 2 shows the procedure of the mesh segmentation for maxillary and mandible tooth separation. First, the Gaussian curvature of each vertex is extracted. The model is then presegmented by threshold using the Gaussian curvature. The threshold segmentation needs to ensure that most region are labeled to be maxillary or mandible teeth except the occlusal contact region. In this study, the threshold is set to be –0.001 empirically. In the occlusal contact region of maxillary and mandible teeth, vertexes may have similar Gaussian curvatures. Thus, only using the Gaussian curvature may fail to segment this region. The average geodesic distance calculates the mean of geodesic distance from each vertex to all other vertexes on the mesh. The value of the average geodesic distance of vertexes in the center of the object is low, and that of vertexes on the periphery is large. To segment the contact region, this study integrates the Gaussian curvature and average geode-

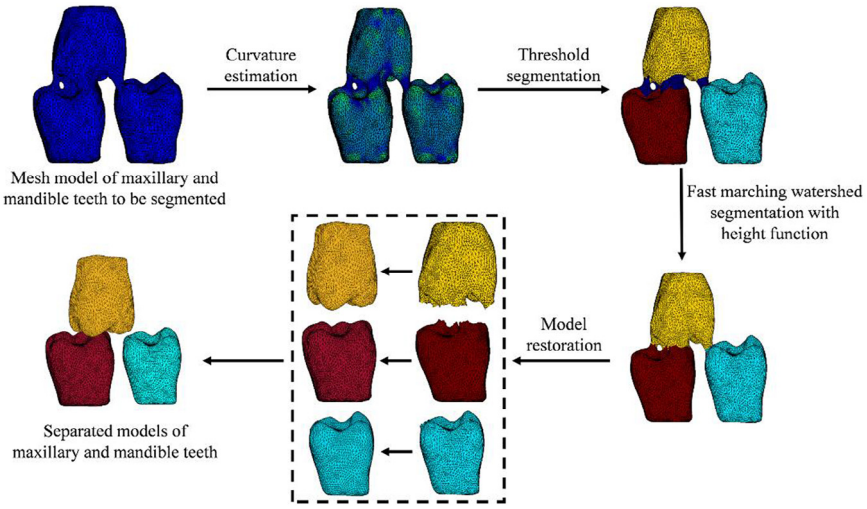

Fig. 2 – Procedure of mesh segmentation for maxillary and mandible tooth separation.

sic distance to construct a height function. The contact region is then segmented and labeled into maxillary or mandible teeth by a fast marching watershed algorithm based on the height function. By integrating the Gaussian curvature and average geodesic distance, when the Gaussian curvature has difficulty to distinguish the maxillary and mandible teeth from the contact region, the height function has a tendency to separate the contact region from the center vertexes.

As the reconstructed model by marching cube algorithm is surface model, there occur holes at the boundary of the separated tooth models. Finally, these holes are restored, and individual complete tooth models are obtained. In order to restore these holes in the separated mesh models, this study first applies the advancing front mesh method to fill the holes of maxillary and mandible teeth independently, and then adjusts the filled holes alternatively to eliminate the possible collision. In the hole filling of each mesh model, the 1-neighborhood vertexes and the corresponding faces of the boundary vertexes are deleted, and holes are filled using the advancing front mesh method [28]. The advancing front mesh method first calculates interior angle at each vertex on the boundary and then finds a vertex which has the smallest angle and creates a new triangle using this vertex.

A collision-free mesh fairing method is used to adjust the filled mesh [29]. A plane is fitted from the new boundary vertexes generated by deleting the 1-neighborhood vertexes and the corresponding faces of the segmented boundary vertexes, and vertexes on the filled mesh are projected to the plane. The interference area and the maximum collision distance that the maxillary and mandible teeth have collided are calculated, and the two corresponding vertexes with the maximum collision distance are marked. For each of the two vertexes, the distance between the vertex and its projection on the fitted plane is calculated and denoted to be 1. Then a parameter α is defined as the proportion of half of the maximum collision distance related to 1. The final coordinates P of vertexes of the filled mesh are determined as follows:

$$P = \alpha P_0 + (1-\alpha) P_1 \tag{18}$$

where P_0 and P_1 denote the corresponding coordinates of vertex on the mesh and projection plane, respectively. The above adjustment procedure iterates alternatively for each of two collided maxillary and mandible teeth until no collision. As the fitted planes of the two teeth will never collide, the adjustment procedure can always guarantee obtaining collision-free tooth models.

4. Experiments and discussions

This study was reviewed and approved by the Institutional Review Board of Shenzhen Institutes of Advanced Technology, Chinese Academy of Sciences. Written informed consents of the subjects were obtained. Cone beam CT (CBCT) volumetric images of ten subjects scanned with natural contacts of maxillary and mandible teeth were used to validate the performance of the proposed method. The scanning parameters of tested images were 120 kV, 5 mA, and with 6 s as time of exposure. Each volumetric image has an isotropic space resolution of 0.25 mm. There are no metal artifacts in these images. Before being segmented, the volumetric images have been reoriented manually so that most slices in the transverse plane contain all the tooth contours.

The manual segmented teeth were used as the "ground truth" and compared to the results of the proposed method. Four metrics were used to quantitatively estimate the segmentation accuracy. The four metrics include two volume overlap metrics, volume difference (VD, mm^3) and Dice similarity coefficient (DSC, %), and two surface distance metrics, average symmetric surface distance (ASSD, mm) and maximum symmetric surface distance (MSSD, mm). VD, DSC, ASSD, and MSSD are defined as:

$$VD = |V_R - V_A|, \tag{19}$$

$$DSC = \frac{2V_R \cap V_A}{V_R + V_A} \tag{20}$$

$$ASSD(S_R, S_A) = mean\{mean\{dist(a, S_R), a \in S_A\}, mean\{dist(r, S_A), r \in S_R\}\} \quad (21)$$

$$MSSD(S_R, S_A) = max\{max\{dist(a, S_R), a \in S_A\}, max\{dist(r, S_A), r \in S_R\}\} \quad (22)$$

where V_R and V_A are the volumes of objects of ground truth and algorithm segmentation, respectively, S_R and S_A are the object surfaces of ground truth and algorithm segmentation, respectively, $dist(a, S_R)$ is the nearest Euclidean distance from a surface point a to the surface S_R, $mean\{\bullet\}$ and $max\{\bullet\}$ are the arithmetical average and maximum operator, respectively.

The presented method was implemented using MATLAB code and ran on a DELL graphics workstation (Win 7, Intel E5-2643 3.3 GHz CPU, 16 GB RAM). The processing time for segmenting the tested images was recorded to assess the efficiency of the method.

4.1. *Qualitative results*

Fig. 3 shows the segmentation results of sample slices by the tooth contour segmentation step based on the Radon transform and the hybrid level set model. In these images, some teeth of maxilla and mandible touch and overlap in slices of occlusal contact area. The visual results indicate that neighboring tooth contours in each jaw are separated successfully, and root contours are well segmented. However, touched maxillary and mandible crowns are failed to be segmented, and there are serious overlap between the segmented contours of maxillary and mandible crowns (in (a)-5—(a)-8 and (b)-1—(b)-(4)).

Fig. 4 shows the 3D models of the teeth generated from the volumetric images in Fig. 3. Models in Fig. 4(a) are directly reconstructed from these segmented tooth contours. In the models, some maxillary and mandible teeth are reconstructed to be one model due to the overlap of segmented contours. After the mesh model segmentation, maxillary and mandible teeth are separated and individual tooth models are obtained (shown in Fig. 4(b), (c), and (d)). These tooth models are visually satisfying and can be manipulated individually to perform digital diagnosis and treatment planning of orthodontics.

Fig. 5 shows the final maxillary and mandible tooth contours of slices in occlusal contact area from volumetric images in Fig. 4 after mesh model segmentation step. Compared to the results in Fig. 3, overlapped maxillary and mandible tooth contours are separated completely, and individual tooth contours are obtained.

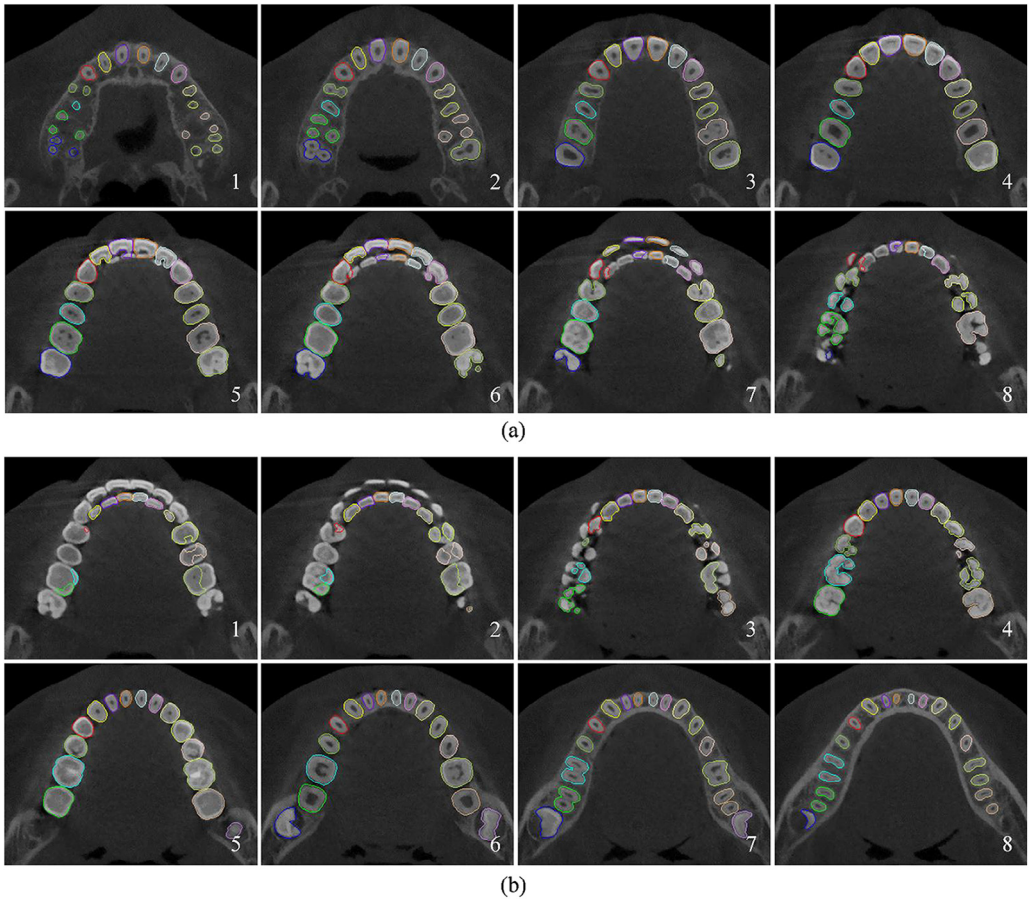

Fig. 3 – Segmentation results of sample slices by the tooth contour segmentation step based on the Radon transform and the hybrid level set model. (a) Results of maxilla, (b) results of mandible. (a)-6 and (b)-1, (a)-7 and (b)-2, and (a)-8 and (b)-3 are respectively the same slice with tooth contact.

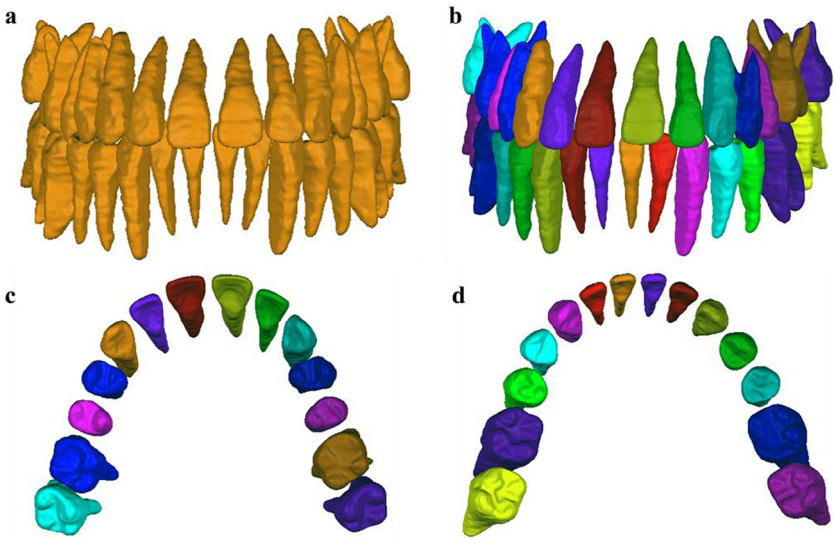

Fig. 4 – 3D models of the teeth generated from the volumetric images in Fig. 3. (a) Tooth models directly reconstructed from the segmented contours. (b) Individual tooth models after the mesh segmentation. (c) Individual maxillary tooth models in (b). (d) Individual mandible tooth models in (b).

4.2. *Quantitative results*

The quantitative segmentation accuracy of the proposed method in terms of all the four types of teeth estimated from the tested volumetric images is listed in Table 1.

As existing automatic and semi-automatic tooth segmentation method cannot extract individual tooth from CT images scanned with contacts of maxillary and mandible teeth, this study did not compare them to the proposed method for the segmentation of these images.

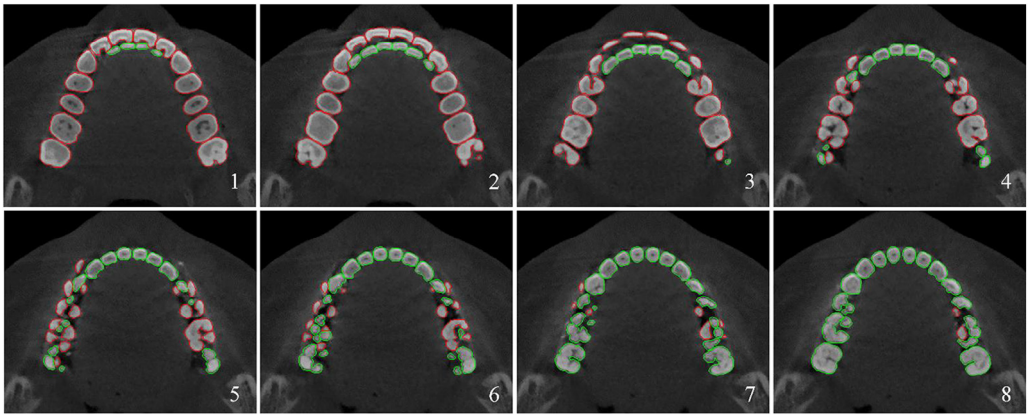

Fig. 5 – Maxillary and mandible tooth contours of slices in occlusal contact area from volumetric images in Fig. 3 after mesh model segmentation step. Red curves mark the maxillary tooth contours, and green curves mark the mandible tooth contours. (For interpretation of the references to color in this figure legend, the reader is referred to the web version of this article.)

Table 1 – Tooth segmentation accuracy of the proposed method for segmenting the volumetric images scanned with natural contacts of maxillary and mandible teeth.

Teeth	Metrics			
	VD (mm^3)	DSC (%)	ASSD (mm)	MSSD (mm)
Incisor	36.94 ± 4.53	90.90 ± 1.74	0.25 ± 0.04	1.30 ± 0.42
Canine	41.31 ± 7.57	90.52 ± 1.59	0.33 ± 0.02	1.28 ± 0.48
Premolar	42.06 ± 6.39	89.94 ± 1.28	0.37 ± 0.05	1.53 ± 0.46
Molar	60.15 ± 15.99	89.15 ± 1.19	0.39 ± 0.18	2.48 ± 0.52

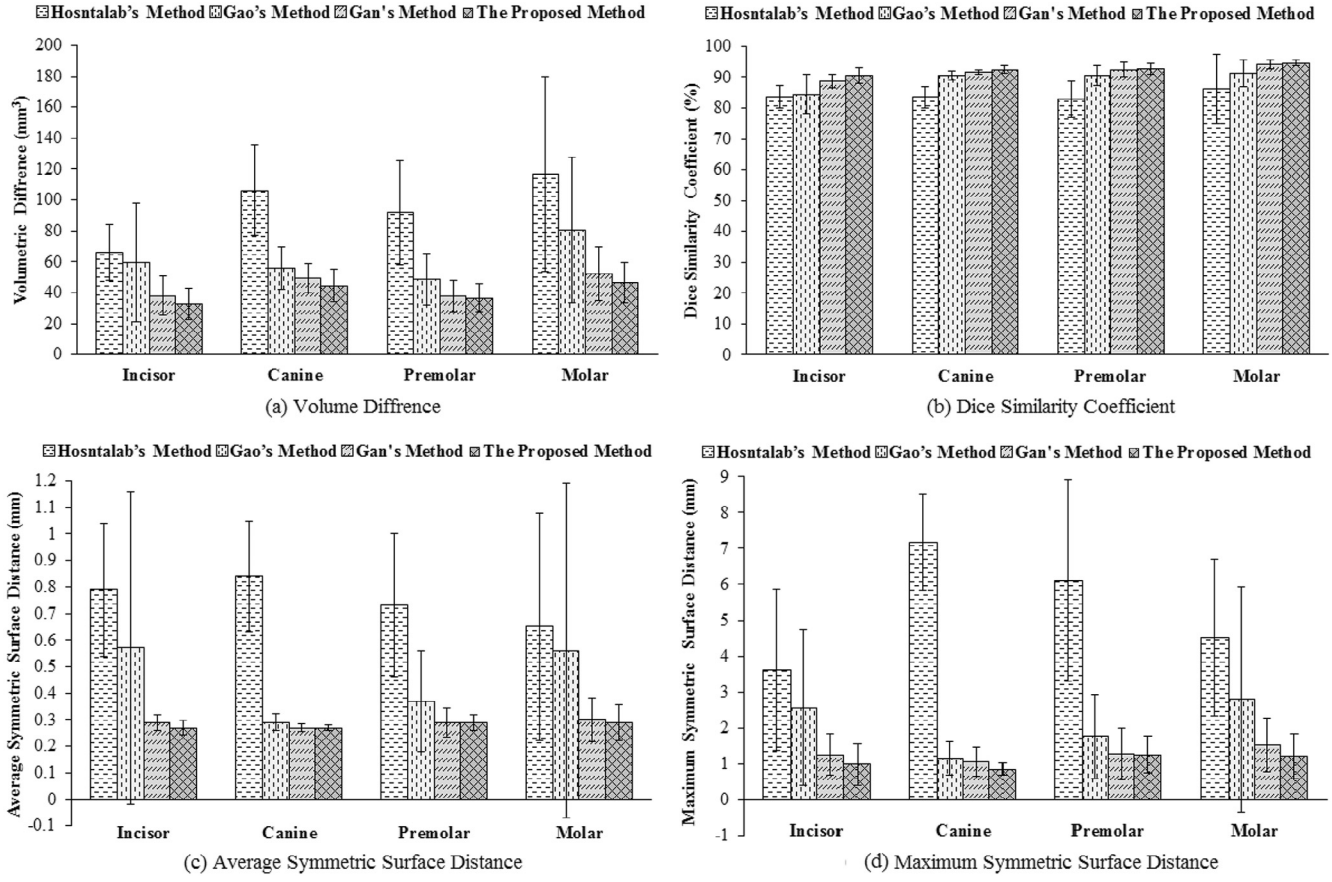

Fig. 6 – Segmentation accuracy comparison of different methods for segmenting volumetric images scanned without any contacts of maxillary and mandible teeth.

4.3. *Computation efficiency*

In the segmentation of tooth contours, the extracted separation line of neighboring teeth makes the segmentation of different teeth in one slice become independent. Thus, different teeth in one slice can be segmented in parallel. This study applied two cores to segment tooth contours in parallel. The computation time of the tooth contour segmentation strategy for segmenting one set of volumetric images is 4.45 ± 0.64 min. The computation time of mesh segmentation for maxillary and mandible tooth separation of one subject is 1.37 ± 0.43 min.

4.4. *Segmentation of CT images scanned without contacts of maxillary and mandible teeth*

The presented tooth contour segmentation step can be directly used to extract individual tooth from CT images scanned without contacts of maxillary and mandible teeth. In order to estimate its performance, sixteen sets of CBCT volumetric images scanned without any contacts of maxillary and mandible teeth were used to test it for crown and root contour segmentation. These images have the same scanning settings with those tested images scanned with natural contact of maxillary and mandible teeth.

The quantitative segmentation accuracy of the presented tooth contour segmentation method has been compared to Hosntalab et al.'s method [4], Gao et al.'s method [10], and Gan et al.'s method [13]. The quantitative comparison results are presented in Fig. 6. Compared to these methods, the accuracy of the proposed method is higher. Statistical significance test showed that there was significant difference ($p < 0.05$) between the segmentation accuracy of the proposed method and Hosntalab et al.'s and Gao et al.'s methods, and there was significant difference ($p < 0.05$) between the segmentation accuracy of the proposed method and Gan et al.'s method for the incisor and molar ($p < 0.05$).

Compared to the three other methods, another advantage of the presented tooth contour segmentation method is that it involves less parameter to be tuned (only one parameter μ) and is more feasible to be applied for clinical application.

4.5. *Limitation of the proposed method*

In clinical orthodontics, the double scanning of the same subject is not allowed, and it is difficult to obtain the images of the same subject scanned both with open bite and close bite positions. Thus, this study applied the manual segmented teeth from images scanned with close bite position as the "ground truth" and compared to the results of the

proposed method. However, a more advisable solution is to use these optically scanning plaster models or intraoral scanning models as ground truth of crowns with occlusion condition. In future works, we will try to collect both the CT images and optically scanning models of same subjects to evaluate the method.

Another limitation is that the hybrid level set model segments 2D tooth contours from the volumetric CT images slice-by-slice, and the segmentation accuracy is somehow dependent on the initial tooth contour. It may fail to segment these angled teeth as there is low coherence between contours of adjacent slices, and the initial tooth contour from the segmented slice may be far from the real contour. To segment the dental CT images with angled teeth, one feasible solution is to manually reorient the volumetric images for different teeth before the segmentation and then map these segmented teeth to the original coordinate space. The future work of this study will focus on the extension of the proposed method for the robustness to angled teeth.

5. Conclusion

This study proposes a method for individual tooth segmentation from CT images scanned with contacts of maxillary and mandible teeth. In the proposed method, tooth contours are first segmented slice-by-slice based on the Radon transform and hybrid level set model. After the tooth contour segmentation, each maxillary tooth whose contours overlap with mandible ones is detected, and a mesh model is reconstructed from all the contours of these maxillary and mandible teeth with contour overlap. Then, the reconstructed mesh models are segmented using threshold segmentation and fast marching watershed algorithm to separate the touched maxillary and mandible teeth. Finally, the separated models are restored to fill holes, and complete individual tooth models are obtained. Experimental results verified that the proposed method successfully segmented individual tooth from tested CT images scanned with natural contacts of maxillary and mandible teeth, and achieved satisfying segmentation accuracy and efficiency.

Conflict of interest

We declare that there is no conflict of interest related to this paper.

Acknowledgments

This work was supported by National Natural Science Foundation of China (No. 61601452), Guangdong Natural Science Funds for Distinguished Young Scholar (No. 2015A030306020), Fundamental Research Program of Shenzhen (No. JCYJ20140417113430639), Youth Innovation Promotion Association, Chinese Academy of Sciences (No. 2015301), and SIAT Innovation Program for Excellent Young Researchers (No. 201302).

REFERENCES

[1] Z. Wei, X. Yu, X. Xu, X. Chen, Experiment and hydro-mechanical coupling simulation study on the human periodontal ligament, Comput. Methods Programs Biomed. 113 (3) (2014) 749–756.
[2] H. Akhoondali, R.A. Zoroofi, G. Shirani, Rapid automatic segmentation and visualization of teeth in CT-scan data, J. Appl. Sci. 9 (11) (2009) 2031–2044.
[3] S.H. Keyhaninejad, R.A. Zoroofi, S.K. Setarehdan, G.H. Shirani, Automated segmentation of teeth in multi-slice CT images, in: 2006 IET International Conference on Visual Information Engineering (VIE 2006), 26–28 September, 2006, pp. 339–344.
[4] M. Hosntalab, R.A. Zoroofi, A.A. Tehrani-Fard, G.H. Shirani, Segmentation of teeth in CT volumetric dataset by panoramic projection and variational level set, Int. J. Comput. Assist. Radiol. Surg. 3 (3–4) (2008) 257–265.
[5] J. Keustermans, D. Vandermeulen, P. Suetens, Integrating statistical shape models into a graph cut framework for tooth segmentation, in: Machine Learning in Medical Imaging, Springer, Nice, France, 2012, pp. 240–247.
[6] L.T. Hiew, S.H. Ong, K.W.C. Foong, Tooth segmentation from cone-beam CT using graph cut, in: Proceedings of the Second APSIPA Annual Summit and Conference (ASC 2010), 14–17 December, 2010, pp. 272–275.
[7] S. Barone, A. Paoli, A.V. Razionale, CT segmentation of dental shapes by anatomy-driven reformation imaging and B-spline modelling, Int. J. Numer. Method Biomed. Eng. 32 (6) (2016) e02747.
[8] H. Heo, O.S. Chae, Segmentation of tooth in CT images for the 3D reconstruction of teeth, in: SPIE Proceedings Vol. 5298: Image Processing: Algorithms and Systems III, SPIE, San Jose, CA, 2004, pp. 455–466.
[9] X. Wu, H. Gao, H. Heo, O.S. Chae, J. Cho, S. Lee, et al., Improved B-spline contour fitting using genetic algorithm for the segmentation of dental computerized tomography image sequences, J. Imaging Sci. Technol. 51 (4) (2007) 328–336.
[10] H. Gao, O. Chae, Individual tooth segmentation from CT images using level set method with shape and intensity prior, Pattern Recognit. 43 (7) (2010) 2406–2417.
[11] H. Yau, T. Yang, Y. Chen, Tooth model reconstruction based upon data fusion for orthodontic treatment simulation, Comput. Biol. Med. 48 (2014) 8–16.
[12] D.X. Ji, S.H. Ong, K.W.C. Foong, A level-set based approach for anterior teeth segmentation in cone beam computed tomography images, Comput. Biol. Med. 50 (2014) 116–128.
[13] Y. Gan, Z. Xia, J. Xiong, Q. Zhao, Y. Hu, J. Zhang, Towards accurate tooth segmentation from computed tomography images using a hybrid level set model, Med. Phys. 42 (1) (2015) 14–27.
[14] L. Wang, K.C. Chen, Y. Gao, F. Shi, S. Liao, G. Li, et al., Automated bone segmentation from dental CBCT images using patch-based sparse representation and convex optimization, Med. Phys. 41 (4) (2014) 043503.
[15] L. Wang, Y. Gao, F. Shi, G. Li, K. Chen, Z. Tang, et al., Automated segmentation of dental CBCT image with prior-guided sequential random forests, Med. Phys. 43 (1) (2016) 336–346.
[16] Y. Guo, A. Şengür, J. Tian, A novel breast ultrasound image segmentation algorithm based on neutrosophic similarity score and level set, Comput. Methods Programs Biomed. 123 (1) (2016) 43–53.
[17] A. Mekhmoukh, K. Mokrani, Improved fuzzy C-means based particle swarm optimization (PSO) initialization and outlier rejection with level set methods for MR brain image

segmentation, Comput. Methods Programs Biomed. 122 (2) (2015) 266–281.
[18] T. Chan, L.A. Vese, Active contours without edge, IEEE Trans. Image Process. 10 (2) (2001) 266–277.
[19] L. Wang, L. He, A. Mishra, C. Li, Active contours driven by local Gaussian distribution fitting energy, Signal Process. 89 (12) (2009) 2435–2447.
[20] T. Chan, W. Zhu, Level set based shape prior segmentation, in: Proceedings of 2005 IEEE Computer Society Conference on Computer Vision and Pattern Recognition (CVPR 2005), 20–25 June, 2005, pp. 1164–1170.
[21] H. Chen, A.K. Jain, Tooth contour extraction for matching dental radiographs, in: Proceedings of the 17th International Conference on Pattern Recognition (ICPR), 23–26 August, 2004, pp. 522–525.
[22] A. Shamir, A survey on mesh segmentation techniques, Comput. Graph. Forum 27 (6) (2008) 1539–1556.
[23] M. Meyer, M. Desbrun, P. Schröder, A.H. Barr, Discrete differential-geometry operators for triangulated 2-manifolds, Visualization and Mathematics III, Springer, Berlin, Germany, 2003, pp. 35–57.
[24] Y. Cheng, Mean shift, mode seeking, and clustering, IEEE Trans. Pattern Anal. Mach. Intell. 17 (8) (1995) 790–799.
[25] D.L. Page, A.F. Koschan, M.A. Abidi, Perception based 3D triangle mesh segmentation using fast marching watersheds, in: Proceedings of 2003 IEEE Computer Society Conference on Computer Vision and Pattern Recognition (CVPR 2003), 18–20 June, 2003, pp. II-27-II-32.
[26] R. Kimmel, J.A. Sethian, Computing geodesic paths on manifolds, Proc. Natl. Acad. Sci. U.S.A. 95 (15) (1998) 8431–8435.
[27] W.E. Lorensen, H.E. Cline, Marching cubes: A high resolution 3D surface construction algorithm, ACM SIGGRAPH Comput. Graph. 21 (4) (1987) 163–169.
[28] P.L. George, É. Seveno, The advancing-front mesh generation method revisited, Int. J. Numer. Methods Eng. 37 (21) (1994) 3605–3619.
[29] N. Qiu, R. Fan, L. You, X. Jin, An efficient and collision-free hole-filling algorithm for orthodontics, Vis. Comput. 29 (6) (2013) 577–586.